On the UV-Visible Light Synergetic Mechanisms in Hybrid Au/TiO2 Model- Nanostructures Achieving Photo-Reduction of Water

Maria-Isabel Mendoza-Diaz, Jérémy Cure, Mehdi Djafari Rouhani, Kui Tan, Sai-Gourang Patnaik, David Pech, Manuel Quevedo-Lopez, Teresa Hungría, Carole Rossi, Alain Estève

On the UV-Visible Light Synergetic Mechanisms in Hybrid Au/TiO_2 Model-Nanostructures Achieving Photo-Reduction of Water

Maria-Isabel Mendoza-Diaz[1], Jérémy Cure[1], Mehdi Djafari Rouhani[1], Kui Tan[2], Sai-Gourang Patnaik[1], David Pech[1], Manuel Quevedo-Lopez[2], Teresa Hungria[3], Carole Rossi[1], Alain Estève[1]*

[1] LAAS-CNRS, University of Toulouse, 7 avenue du colonel Roche, 31031 Toulouse, France

[2] Department of Materials Science and Engineering, University of Texas at Dallas, Richardson, TX (USA)

[3] Centre de Microcaractérisation Raimond Castaing, 31000 Toulouse, France

ABSTRACT:

This paper reports the synergetic effects of UV and visible light irradiation on the photocatalytic activity of well-defined nanostructures composed of TiO_2 films and Au nanoparticles. New insights into the electronic as well as the chemical processes that drive water decomposition were obtained by varying the position of the NPs on top and at different depths inside the semiconductor film. This work highlights a synergetic effect of UV and visible light on the photocatalytic activity of all the Au containing structures: hydrogen produced under UV+Vis shows an 100 % enhancement compared to the net production obtained only under UV or vis light. The systems where Au NPs are embedded in the TiO_2 outperform the one where NPs are positioned on the surface, indicating that water-splitting reaction occurs primarily on the TiO_2 surface rather than on the metal. Photocurrent and photocatalytic activity measurements under UV (353–403 nm), visible (400–1100 nm) and UV+Vis (300–1100 nm) light, revealed the synergetic contribution of UV and Vis. Indeed, the plasmonic Au NPs create an intense oscillating electric field at the Au NPs/semiconductor interface (visible light contribution); this mechanism coupled with the

Schottky barrier formation generates hot electrons resulting in better photo-excited charge separation. In addition, contrary to what is generally assumed, charges injection by the plasmon from the metal into the semiconductor play a marginal role in the Hydrogen Evolution Reaction (HER). Furthermore, the paper highlights the positive impact of the semiconductor crystallinity surrounding the metal particles to avoid the charge carrier recombination; and the importance of a surface free of oxygen vacancies, whose presence can inhibit the water decomposition.

1. INTRODUCTION

Hydrogen energy carriers play a central role in the energy transformation required to limit global warming.[1-2] In this frame, photocatalysis, *i.e.* unbiased water splitting using sunlight water without any electric source, counter electrodes or supporting electrolyte,[3-7] rigorously offers one of the most promising solutions to produce green and clean hydrogen.[8-9] In this case, the photocatalyst, mostly a powder, dispersed in an aqueous solution is irradiated with sunlight, and hydrogen is produced[3, 10-13] Hence, an efficient photocatalyst should exhibit good absorption of sunlight, achieve adequate photo-generation of charge carriers with low recombination, and possess suitable positions of the valence and conduction bands with respect to the chemical potentials of water splitting. Titanium dioxide (TiO_2) remains a benchmark photocatalyst with high stability, low cost, and low toxicity, but it is active only in the ultra-violet (UV) spectra and the rate of recombination of photo-generated charges (electron/hole pairs) is high.[14] Thus, for practical applications, the photocatalytic reactions are inhibited under sunlight. Several engineering approaches based on structural and chemical modifications, have been explored to overcome some of the drawbacks mentioned above and to enhance the photocatalytic activity of TiO_2. For example, creating heterojunctions, doping with metals and/or non-metals and/or using dye additives,[15-20] have proved to be effective in slightly enhancing the absorption spectrum under visible light (vis)[21-22] or avoiding recombination of

charges due to their chemical affinity or by electronic means such as the presence of a Schottky barrier that serves as a charge trap.[19,20] Along the same line, one of the main research axes focuses on combining the TiO_2 photocatalyst with plasmonic-metal nanostructures such as gold nanoparticles (Au NPs). Several Au/TiO_2 hybrid structures (mostly nanopowders) have shown great potential for photocatalytic solar conversion applied to photodegradation of dyes,[23] or oxidation reactions such as methanol or cyclohexane oxidation.[24-25] While a more conceptual understanding is reported in literature, the documentation related to the determination and quantification of the various mechanisms (electronic and chemical) acting under UV + Vis irradiation is still sparse with no real consensus on their origin. Under UV, some authors observed that Au NPs act as an electron reservoir, facilitating charge separation and thus enhancing the photocatalytic process.[23] This led also to the conclusion that hydrogen could be produced at the metal surface.[26] On the other hand, it has been suggested that under visible light, plasmonic excitation leads to electron injection from the metal into the semiconductor conduction band.[27] Other authors mention that the plasmonic effects generate electron-hole pairs in the semiconductor, which would result in a different distribution of charges into the hybrid TiO_2/Au systems.[28] Although synergetic effects in Au/TiO_2 nanocatalysts under UV+Vis irradiation were macroscopically observed[14, 23, 26, 29-31] and even optimized in certain cases,[23] the electronic mechanisms derived from UV+Vis interaction still remains elusive.

Our study seeks to get further insights into this synergetic effect under UV+Vis irradiation and assess the plasmonic contributions on direct photocatalytic hydrogen production by evaluating the role of UV, visible light and both, supported by Electric Field Simulation and photocurrent measurements. For this purpose, different well-defined Au/TiO_2 model-structures were prepared by decorating a sputtered TiO_2 thin film with Au NPs and/or by embedding them at different depths in the TiO_2. A full structural, chemical, optical and photoelectrochemical characterization was

performed on each of the Au/TiO_2 structures. The measurement of their photocatalytic activity was investigated by measuring the hydrogen produced under UV (353–403 nm), visible (400–1100 nm) and UV+Vis (300–1100 nm) light. Under UV, we demonstrated the role of the Schottky barrier between the metal/semiconductor, which allows the trapping of photo-excited holes and improves the charge separation in the overall system. Under visible light, we evidenced the presence of both a plasmonic electric field and the generation of hot electrons in TiO_2. However, the latter does not affect H_2 production, because of a high recombination rate. Importantly an enhancement (× 500) of the hydrogen evolution reaction (HER) is seen under both UV+Vis light. The contributions: being the UV photoexcited charges into TiO_2, the Schottky barrier formation and effects associated to the intense electric field of SPR, elucidate the synergistic contribution of UV and Vis light on these hybrid nanostructures. Notably the energy transfer generated by the intense electric field contributes to the promotion of UV excited electrons in TiO_2 to reach the surface, enhancing hydrogen production. But more importantly, this work invalidates to some extent the role of plasmonic nanoparticles as charge injectors into the semiconductor. In addition, the experimental work showed that the chemical decomposition of water does not occur primarily on the Au NPs surfaces, in contradiction with what is often suggested in literature.[32-33] Finally, it was determined that the degree of oxidation of TiO_2 impacts negatively on the HER.

2. EXPERIMENTAL SECTION

2.1. Sample Preparation. A first layer of TiO_2 (270 nm-thick) was sputter-deposited by direct current magnetron sputtering on glass substrates. The Au NPs were synthesized on the TiO_2 by a photo-deposition process under UV irradiation (365 nm, 100 W, 30 min) using gold chloride trihydrate (III) acid ($HAuCl_4.3H_2O$, ≥99.9%, Sigma-Aldrich, CAS: 16961-25-4) aqueous solution

(50 mL, 2.5 × 10^{-4} mol/L), a stabilizing agent of trisodium citrate dihydrate ($Na_3C_6H_5O_7.2H_2O$, 99.0%, Alfa Aesar, CAS: 6132-04-3) solution (5 mL, 0.05 mol/L) and ethanol (99.9%, Technic, CAS: 64-17-5) as a sacrificial agent (5 mL).[34-35] An annealing step under air at 200 °C during 10 min allowed the grafting of the NPs on the TiO_2 layer. The stabilizing agent was removed after rinsing with deionized water. Next, a second TiO_2 layer (15 and 270 nm thickness for different samples) was deposited by direct magnetron sputtering as previously described. More experimental details are described in the Supporting Information, SI, Section A-1. Analytical grade chemicals were used as received. All solutions were made using DI water obtained from Milli-Q (Millipore) system.

2.2. Characterization. The characterization methods included scanning electronic microscopy (SEM, FEI Helios 600i Nanolab), high-angle annular dark-field scanning transmission electronic microscopy (HAADF-STEM, FEI Helios Nanolab), energy dispersive X-ray spectrometry (EDS), grazing incidence X-ray diffraction (GI-XRD, Bruker D8 Discover system) X-ray photoelectron spectroscopy (XPS, ESCALAB 250 X-Ray photoelectron spectrometer), Electron Energy Loss Spectroscopy (EELS) was carried out in STEM mode and UV-vis spectroscopy (Perkin-Elmer Lambda 950 UV-vis spectrometer). Note that the surface morphology of TiO_2 was characterized by atomic force microscopy (AFM) using Veeco equipment (Dimension 3100) with tapping mode. For photocatalytic experiments, 1 cm^2 samples were placed into a quartz reactor (60 mL) filled with an aqueous solution (10 mL, 35% v/v ethanol) and connected to a gas chromatography apparatus (GC, Perkin-Elmer Clarus 580) in order to monitor the hydrogen production (Figure S1). The sample was irradiated by a Xenon light lamp (Cermax® PE300B-10F) equipped with optical filters to delimit the spectral region. The relative spectral distribution of the Xenon lamp is given in Figure S2. The quantity of released hydrogen was monitored every 6 h and the hydrogen production rate was calculated after 24 h. The photoelectrochemical measurements were carried

using a VMP-3 and a VSP Biologic potentiostat with a three-electrode setup. For each working electrode, the respective sample was deposited onto a glass coated with Ti/Au (100 and 300 nm). The counter electrode was a platinum net and a silver chloride electrode (Ag/AgCl) was used as reference. An aqueous 0.5 M solution of sodium sulfate anhydrous (Na_2O_4S, >99%, Fluka, CAS: 7757-82-6) was used as electrolyte. The electrochemical cell was irradiated with an optical fiber wire (Eurosep Instruments) connected to the previous mentioned Xenon light lamp. More experimental details are described in SI, Sections A-2 and A-3.

2.3. Electric Field Simulation. Simulations were carried out using the discrete dipole approximation-based (DDA) open-source DDSCAT software package (see SI, Section A-4). The Au/TiO_2 model-structures were built considering a 15 nm diameter Au nanoparticle. The three hybrid models were 1) a Au NP deposited on a TiO_2 surface, thereafter *Au-surface*; 2) a 5 nm thick conformal TiO_2 covering a Au NP, thereafter *Au-subsurface*; and 3) a Au NP fully embedded into the TiO_2 matrix, thereafter *Au-embedded*. The three model-systems were irradiated, normal to the TiO_2 surface, at 550 nm corresponding to the maximum plasmonic resonance wavelength of the bare gold nanoparticle. All structures were bathed in a water medium (1.33 refractive index).

3. RESULTS AND DISCUSSION

3.1. Structural and Optical Characterization. To investigate plasmonic and non-plasmonic contributions of the NPs on the water splitting reaction, various TiO_2/Au structures were fabricated by alternatively depositing films of TiO_2 and Au NPs as illustrated in Figure 1 (left column). Strictly, comparing different model systems is a complex task, as some conflicting parameters may impact the results. For instance, the change of the TiO_2 thickness induces a variation on the film roughness and crystallinity (see SI, Section B-1) which can highly influence the photocatalytic

efficiency. Therefore, a fixed thickness was kept for all samples to ensure the surface roughness and anatase/rutile phase ratio. A TiO_2 film of 270 nm was chosen as the reference for its highest hydrogen production as previously reported.[36] As seen in the SEM images in Figure 1a, the TiO_2 thin film has a columnar morphology, which is rather disordered, with grain sizes from ~20 to 50 nm, accompanied by the presence of porosities (~1-10 nm) between the columns. This is in accordance with the morphology generally observed in TiO_2 films deposited by vapor deposition.[37] For the sample Au-on-TiO_2 (Figure 1b), Au NPs were deposited on top of the TiO_2 surface with an areal density of 60 ± 1 NPs/μm². The photo-deposited Au NPs are spherical with a size range of 30-70 nm (insert in Figure 1b). The size dispersity is closely related to the geometrical constraints imposed by the roughness of the TiO_2 structure. Therefore Au NPs of different sizes were located at different depths between the semiconductor columns as discussed in a previous study.[34] The HAADF-STEM observations indicated that smallest Au NPs (~7 nm in size) are also into the TiO_2 porosities. This probably results from the decomposition and constrained agglomeration of some gold precursors within the porosities during the photo-deposition process (Figure 1b-d).

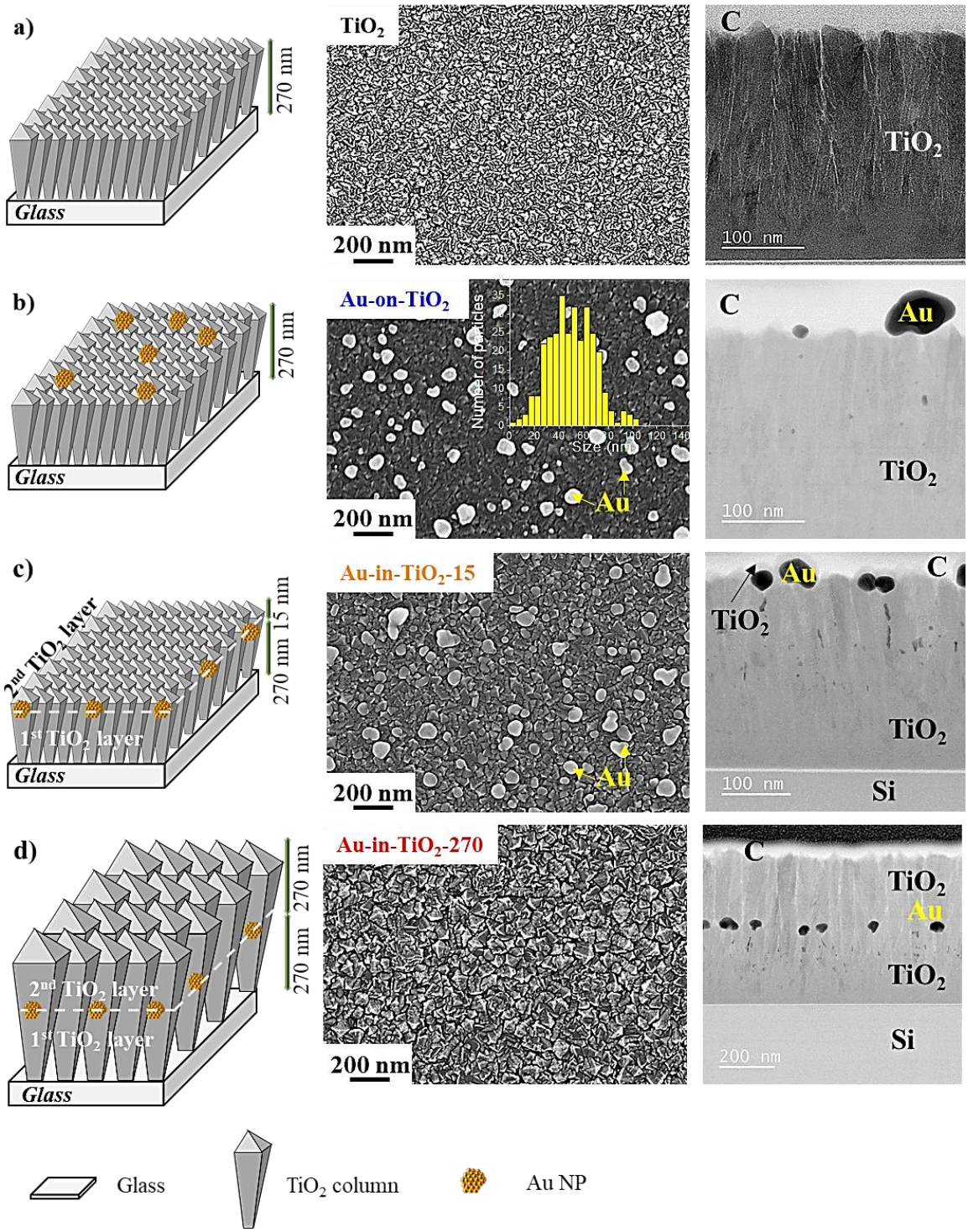

Figure 1. *(Left) Schematic illustrations of TiO_2 and TiO_2/Au hybrid structures. (Middle) SEM images of the samples surface area. (Right) HAADF-STEM cross-section images: a) TiO_2 thin film; b) Au-on-TiO_2 (inset of the Au NPs size dispersion in yellow); c) Au-in-TiO_2-15 and d) Au-in-TiO_2-270. Letter C corresponds to a top layer of protective sputtered carbon.*

The Au-in-TiO_2-15 and -270 structures (Figure 1c and d) were fabricated by depositing a TiO_2 film of 15 and 270 nm on top of the Au-on-TiO_2 structure, respectively. In these samples the second layer of TiO_2 completely covers the nanoparticles (SEM and HAADF-STEM cross-sections in Figure 1c and d, and SI, Section B-2.1). This was also confirmed by EDS spectroscopy (see SI, Section B-2.2). Note that the TiO_2 grains sizes increased from 20-50 nm to 35-80 nm in the second TiO_2 deposited layer, this is related to the regrowth process where the columnar features continue their propagation across the TiO_2/TiO_2 interface as observed in the HAADF-STEM cross-section (Figure 1d).

The GI-XRD patterns of the three structures further confirmed their compositions, the TiO_2 matrix was composed by 84 ± 1% and 16 ± 1% of anatase and rutile phases, respectively (Figure 2a). The Au peak intensities decreased progressively for Au-in-TiO_2-15 and Au-in-TiO_2-270, compared to Au-on-TiO_2. In addition, the anatase/rutile ratio was not affected by the short annealing step that follows the NPs photo-deposition. XPS results (Figure 2b-d and SI, Section B-2.3) were consistent with XRD and SEM observations. The TiO_2 signature was clearly identified from O 1s and Ti 2p energy levels. Au 4f peaks were clearly observed for the Au-on-TiO_2 sample. The Au signature completely disappeared when Au NPs are embedded into the TiO_2. A slight Ti 2p peak shift (-0.2 eV) was observed for Au-in-TiO_2-15 and Au-in-TiO_2-270 (Figure 2c, see SI, Section B-2.3, Table S1). This is explained by the interactions between the Au and TiO_2 that affect the Ti-O bonds by lowering Ti 2p binding energy.[38]

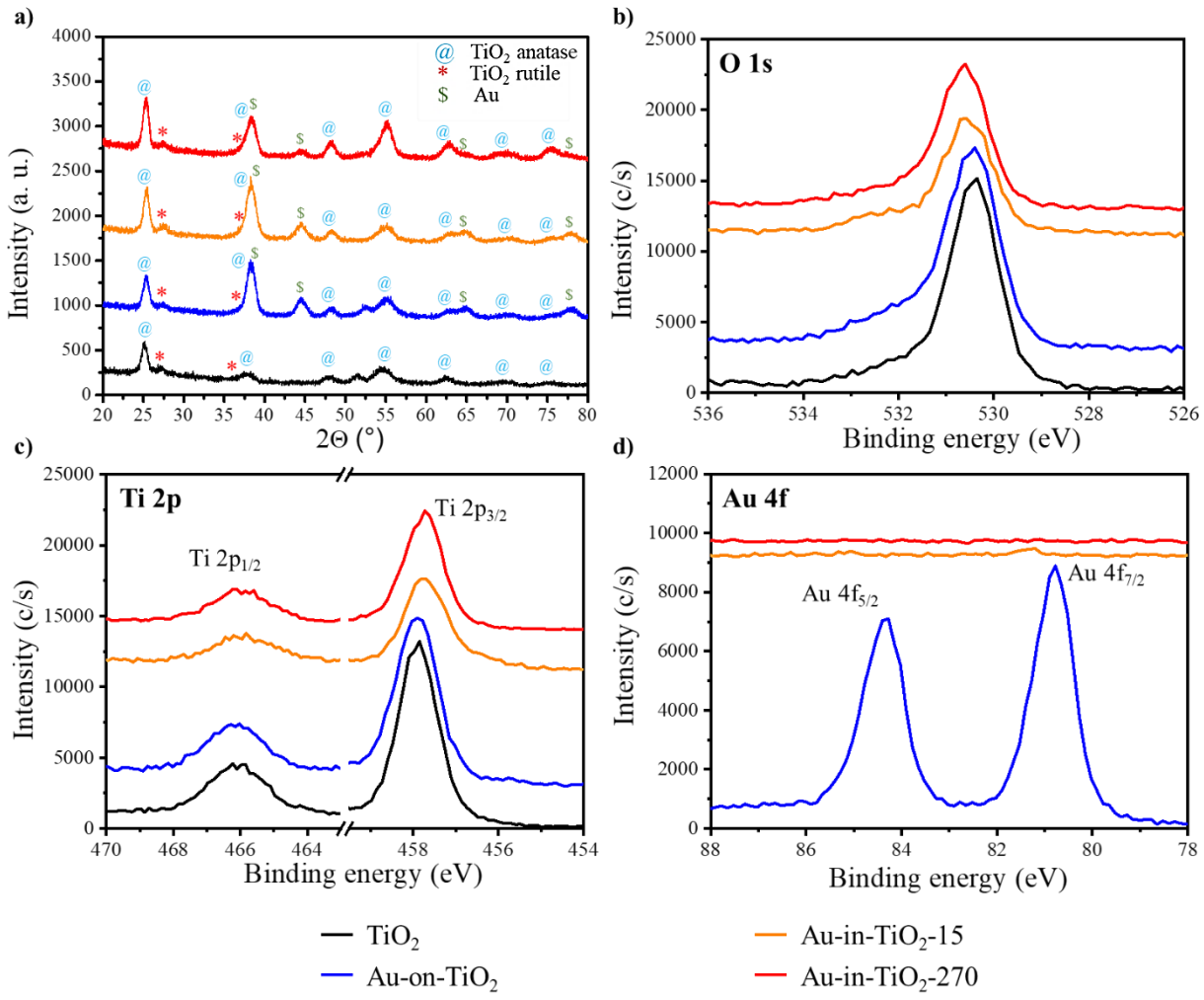

***Figure 2**. GI-XRD patterns and XPS spectra for TiO_2* (black curve) and *Au/TiO_2 hybrid structures; a) GI-XRD peaks are labelled by anatase-TiO_2 (blue @), rutile-TiO_2 (red *) and Au (green $); b) O 1s; c) Ti $2p_{1/2,3/2}$ and d) Au $4f_{5/2,7/2}$ regions.*

The transmittance of the three structures was evaluated by UV-vis spectroscopy (Figure 3a). The transmittance was null from 350 to 200 nm because of the total absorption of light by TiO_2 (Figure 3a, black curve). The ripples in the 400-850 nm range corresponded to the constructive and destructive interferences related to the film thickness and the difference of the refractive index between the TiO_2 film and the glass substrate.[39] Because of these ripples, the analysis of the absorption properties of the materials is quite difficult. However, the TiO_2 film alone did not show

a significant absorption in the range of 450-700 nm and the Au-on-TiO_2 structure showed an enhancement of its absorption in the visible light range (450-700 nm region) (Figure 3a, black and blue curves). This phenomenon can be attributed to the LSPR of Au NPs and its coupling with the local dielectric field of the semiconductor environment.[28, 40-41] This is consistent with the further red-shifting of the absorption observed for Au-in-TiO_2-15 and Au-in-TiO_2-270 in the 450-700 nm spectrum. Indeed, the addition of a 15 nm-thick TiO_2 layer (Au-in-TiO_2-15) induced a red-shift of the absorption (around ~600 nm) whereas the major ripples were only slightly red-shifted (Figure 3a, orange curve). With a thicker film covering the Au NPs (Au-in-TiO_2-270) the red-shift was even more important i.e. localized around 650 nm, (Figure 3a, red curve). To summarize, all Au containing structures exhibited absorption in the visible light as expected. While it is hard to make a hierarchy of absorption levels between the different Au/TiO_2 systems, the absorption band of the plasmonic peak seemed to shift to higher wavelengths for the Au-in-TiO_2 samples.[28]

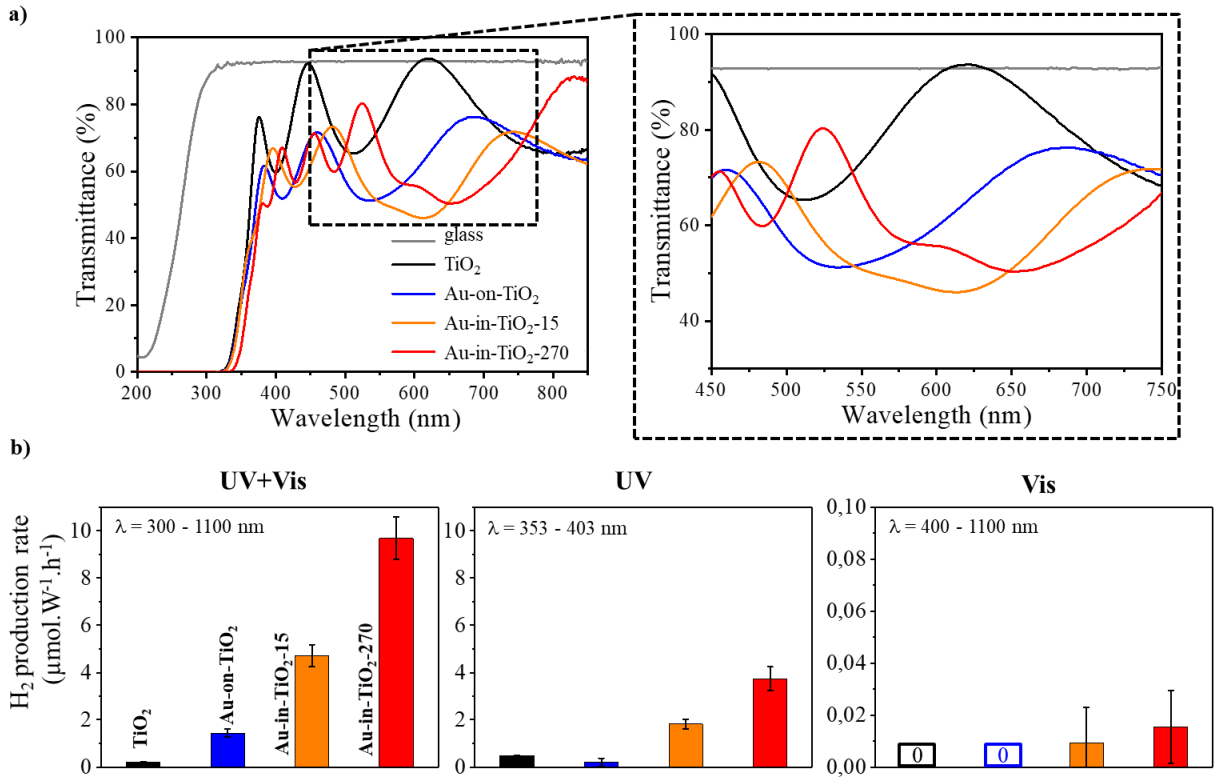

Figure 3. *a) UV-visible absorption spectra (in transmission) of TiO_2, Au-on-TiO_2 and Au-in-TiO_2 in the 200-850 nm (left) and 450-750 nm (right) regions. Note that the transmittance of glass is depicted in grey. b) normalized H_2 production rate per light flux and surface area of TiO_2, Au-on-TiO_2 and Au-in-TiO_2 structures. The samples were irradiated under UV+Vis light (300-1100 nm, left), UV light (353-403 nm, middle) and visible light (400-1100 nm, right): TiO_2 (black curve and bar), Au-on-TiO_2 (blue curve and bar), Au-in-TiO_2-15 (orange curve and bar) and Au-in-TiO_2-270 (red curve and bar).*

The photocatalytic hydrogen production of these structures was evaluated in a 35% v/v ethanolic aqueous solution under irradiation of UV+Vis (300-1100 nm), UV (353-403 nm) and visible (400-1100 nm) light. The HER rate was calculated after 24 h of irradiation and normalized with respect to the incident light flux on the sample. A correction for the light flux was done when UV and

visible filters were used (see SI, Section B-3.1). Note that the hydrogen release rate remains constant in time (see SI, Section B-3.2).

For UV irradiation the production rates for reference TiO_2, Au-on-TiO_2, Au-in-TiO_2-15 and Au-in-TiO_2-270, were 0.5, 0.1, 1.8 and 3.7 $\mu mol.W^{-1}.h^{-1}$, respectively (Figure 3b). Whereas for visible, the production rate for TiO_2 and Au-on-TiO_2 was zero, and a poor rate of 0.0092 and 0.0155 $\mu mol.W^{-1}.h^{-1}$ was obtained for Au-in-TiO_2-15 and Au-in-TiO_2-270, respectively. According to this, a first observation is that, under UV light, the systems exhibits a higher H_2 production rate than under Vis light. Also, under UV, the systems with Au NPs show a clear enhancement compared to the TiO_2 reference (Figure 3b). A second observation is that the H_2 production rate increases drastically for Au/TiO_2 structures when they are exposed to the UV+Vis compared to reference TiO_2. The measured HER rates reached 1.4, 4.7 and 9.7 $\mu mol.W^{-1}.h^{-1}$, for Au-on-TiO_2, Au-in-TiO_2-15 and Au-in-TiO_2-270, respectively, whereas the HER for plain TiO_2 was 0.2 $\mu mol.W^{-1}.h^{-1}$. This corresponds to an enhancement factor of 7, 23 and 48 for Au-on-TiO_2, Au-in-TiO_2-15 and Au-in-TiO_2-270, respectively, with respect to TiO_2.

Primarily, these results evidence that the direct contact between water and Au nanoparticles is not critical to catalyze the photo-reduction of water, which suggests that the water splitting reaction takes place mostly onto the semiconductor surface. Primarily, these results evidence that the direct contact between water and Au nanoparticles is not critical to catalyze the photo-reduction of water, which suggests that the water splitting reaction takes place mostly onto the semiconductor surface. Next, a crucial understanding between the respective role of UV versus visible light in the HER in the three Au/TiO_2 systems must be addressed. It is known that the band bending resulting from the Schottky barrier between the metal and the semiconductor can enhance the photocatalytic activity compared to the bare semiconductor. Upon UV irradiation electron-hole pairs are generated in TiO_2, next, due to the band bending associated to the Schottky barrier presence, holes located in

the valence band of the TiO_2 are attracted towards the metal NPs where they are annihilated by electrons. This recombination prolongs the lifespan of the electron in the conduction band of TiO_2. This is consistent with the H_2 production rate data (Figure 3b) were the best photocatalytic activity was obtained for the nanostructures where the metal-semiconductor junction is present, such as Au-on-TiO_2 and Au-in-TiO_2. On the other hand, the plasmonic resonance effects of Au nanoparticles that take place under visible light also play an important role in the charge transport mechanisms. As surface plasmon resonance creates a collective oscillation of conduction electrons at the interface between the Au and the TiO_2, Plasmon Resonance Energy Transfer (PRET) in the vicinity of the NPs and production of hot electrons in the metal are possible.

To shed light on these mechanisms, DDA simulations were performed to model the intensity and distribution of plasmonic near-fields in the three model-systems: *Au-surface*, *Au-subsurface* and *Au-embedded*, corresponding to the three Au/TiO_2 experimented structures (see SI, Section B-4). We can observe that the structures with embedded Au NPs exhibited a more intense electric field in the vicinity of the TiO_2 surrounding the Au NP. Notably in the normal axis to the incident light, an axisymmetric electric near-field enhancement due to plasmonic effect exhibited four times more intensity for *Au-subsurface* and *Au-embedded* systems (55 and 53 intensity enhancement respectively), than that of *Au-surface* giving an intensity enhancement of 13 (Figure 4).

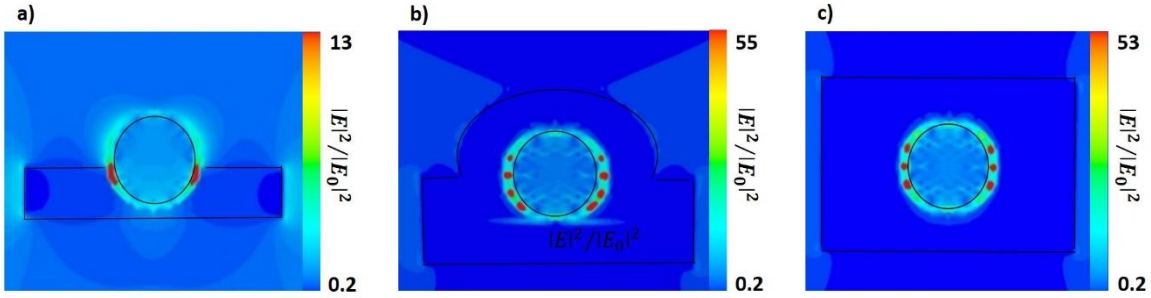

Figure 4. *Cross-sections giving the electric near-field intensity enhancement* ($|E|^2/|E_0|^2$, E *accounts for the calculated electric near field while* E_0 *is the incident electric field) for the three Au/TiO₂ simulated systems: (a) Au-surface corresponding to Au-on-TiO₂, (b) subsurface Au corresponding to Au-in-TiO₂-15, (c) embedded Au corresponding to Au-in-TiO₂-270. The Au is 10 nm in diameter. The solid black lines underline the Au and TiO₂ regions contours.*

Now, comparing *embedded-Au* and *subsurface-Au* structures, not only the intensity, but also the spreading of the maximum intensity regions were wider than that of the *Au-on-TiO₂* model system, pleading for a variation of the plasmonic intensity with increasing Au depth. Note that these results are in accordance with simulations on Janus-type nanoparticular systems.[28] Unfortunately, the size limitation in simulations does not allow to rule quantitatively the issue of depth variation and to address the experimental findings, *i.e.* Au-in-TiO_2-270 structure outperforms the Au-in-TiO_2-15 sample in terms of hydrogen production rate: 7.7 $\mu mol.W^{-1}.h^{-1}$ against 1.8 $\mu mol.W^{-1}.h^{-1}$, under UV, whereas photocurrent (not shown) are rather the same for both structures under UV. To address this point, the chemical composition of TiO_2 in the vicinity of the Au NPs was analyzed for Au-in-TiO_2-15 by energy electron loss spectroscopy (EELS) which is particularly appropriate to monitor the evolution of the oxidation state of oxides. Scans are provided in Figure 5a. The spectra of Ti L_3 and L_2 edges at ~455 eV and ~465 eV were acquired near a Au NP and along the TiO_2 interface, *i.e.* starting in the first 270 nm TiO_2 layer and finishing into the top TiO_2 layer (line scan of ~20 nm). The spectrum taken inside the first TiO_2 layer (Figure 5a, spectrum 2) clearly shows the two dominant split peaks (Ti $L_{2,3}$-edges@455-465 eV and O *K*-edges@530 eV) corresponding to the TiO_2-anatase (Ti^{4+}).[42] The spectrum taken from the top layer of Au-in-TiO_2-15 is quite distinct (Figure 5a, spectrum 1): two peaks can be distinguished in the L_3-edge with a higher energy peak being somewhat asymmetric and no split. The titanium oxide corresponds to a Ti_2O_3 with a low

valence state (Ti^{3+}).[42] The presence of such oxygen vacancies revealed a defective layer that could explain why the H_2 production rate decreased for this sample, either by inhibiting the surface chemical process of the photo-reduction of water, or by enhancing undesirable charge recombination on these defects. With the aim to increase the coordination state of the surface/subsurface layers in the Au-in-TiO_2-15 sample, without any chemical modification of the 270 nm TiO_2 underneath layer, the sample Au-in-TiO_2-15 was annealed at 200 °C under air during 10 min and characterized again using EELS (a-Au-in-TiO_2-15, Figure 5b. Upon annealing, the 15 nm top layer (Figure 5b, spectrum 3) showed the signature of anatase very close to that of the 270 nm TiO_2 layer, corresponding to the Ti^{4+} valence state (Figure 5a, spectrum 2). In addition, the chemical composition of the first 270 nm layer was not modified upon annealing (Figure 5b, spectrum 4). The annealing lowers the oxygen vacancy concentration by local recrystallization of the oxide.[42-43] The photocatalytic performance of the annealed Au-in-TiO_2-15, was measured in the same conditions under UV+Vis light (see SI, Section B-5) is now equivalent to that of Au-in-TiO_2-270. Indeed, the HER rates normalized with respect to the light flux received by the sample is now 9.1 $\mu mol.W^{-1}.h^{-1}$ (Au-in-TiO_2-270 gives 9.7 $\mu mol.W^{-1}.h^{-1}$, Figure 5c). Two important conclusions can be derived from these results. The titanium dioxide stoichiometry and the defective nature and quality of the interface close to the Au NPs influence greatly the rate of recombination of the photo-induced charges. In addition, Ti^{3+} surface sites show a penalizing effect on the photo-reduction of water.

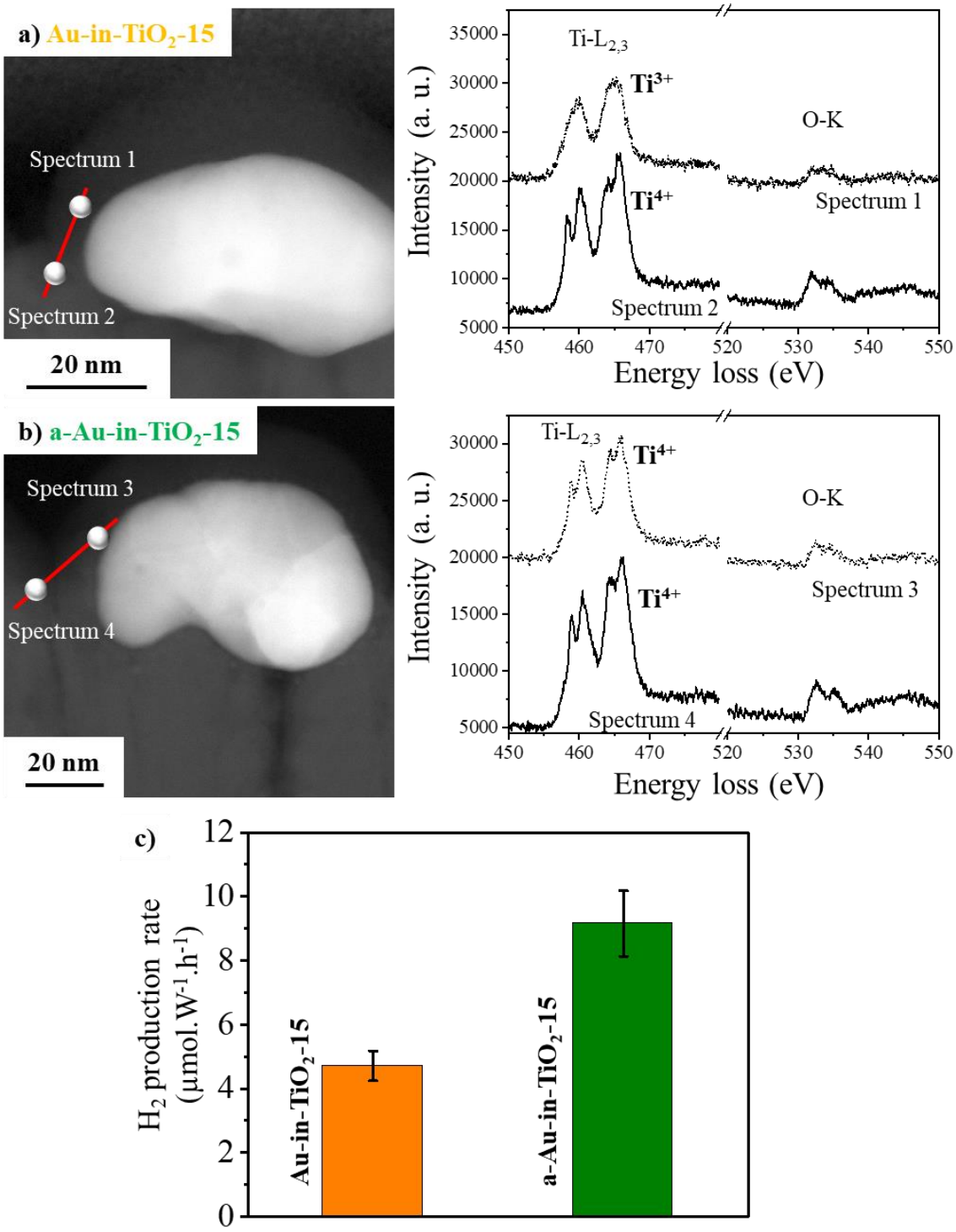

Figure 5. *The EELS analysis is performed along the red line depicted in the STEM images for: a) Au-in-TiO_2-15 and b) annealed a-Au-in-TiO_2-15. EELS core loss edges are background subtracted*

using a power law fit before being plotted. c) Normalized H_2 production rate under UV+Vis for: Au-in-TiO_2-15 (orange bar) and annealed Au-in-TiO_2-15 (noted a- Au-in-TiO_2-15, green bar).

3.2. Transport Mechanisms of Photogenerated Charges. All the Au/TiO_2 structures exhibit a UV+Vis synergetic effect, *i.e.* when the full spectrum is used, the hydrogen production rate roughly doubles compared to UV exposure while, under visible light only, H_2 production is negligible. A similar trend was observed in the study by Yan et al.[26] where Au NPs of various sizes (~3 to 10 nm range) were deposited on top of a TiO_2 anatase substrate. This raises questions on the exact role and impact of plasmonic effects of the Au NPs on the photocatalytic hydrogen production. For what concerns plasmon-induced charge generation, photoelectrochemical measurements were conducted in a cell containing a 0.5 M Na_2SO_4 solution using a three-electrode system with a Pt counter electrode and Ag/AgCl as reference electrode. Photocurrent response under visible light was tested to evaluate the response of the Au NPs in the different structures. The chronoamperometric I-t curves obtained under a pulsed irradiation at 0 V (vs. Ag/AgCl) are shown in Figure 6a. Contrary to the HER results under visible light showing no hydrogen production, all Au-containing samples exhibited a notable photocurrent and its response with the on-off cycles was highly reproducible. Note that the hierarchy in the photocurrent intensity agrees well, qualitatively, with hydrogen production, and also with the simulated intensity of the plasmonic near field; the Au-in-TiO_2-270 sample showed the highest photocurrent followed by the Au-in-TiO_2-15 and Au-on-TiO_2 with a photocurrent of ~4.3, 2.1, 1.2 $\mu A.cm^{-2}$, respectively (see Figure 6a). Note that, even though electrons are being generated under visible light as demonstrated by photocurrent measurements, their conversion into hydrogen molecules is not observed as seen from HER experiment (see Figure 3b).

Additionally, as the majority of charges present in the system emanate from the UV contribution, to corroborate the recombination rate in the samples with least and highest HER, *i.e.* TiO_2 and Au-in-TiO_2-270, linear sweep voltammetry curves (Figure 6b) were obtained under dark and UV+Vis light to extract the flat-band potential. For semiconductor materials, negative flat-band potentials are obtained when the separation of the photogenerated hole-electron becomes more easier, favoring the transfer of electrons to reduce H^+ to H_2.[44] As expected, the value for Au-in-TiO_2-270 was -0.58 V (vs. Ag/AgCl), which is more negative than that of TiO_2 that was -0.18 V (vs. Ag/AgCl).

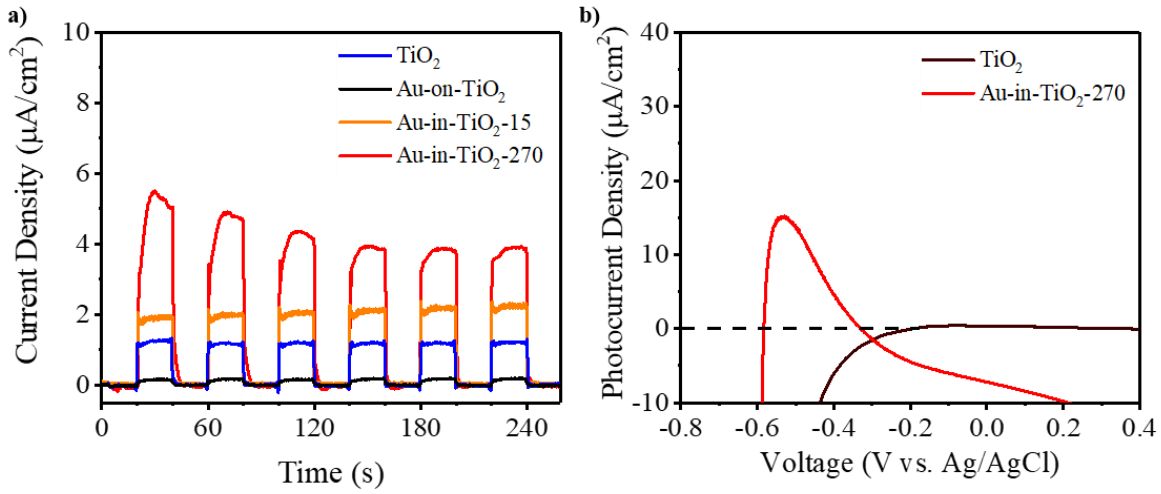

Figure 6. *a) On/off photocurrent measurements on TiO_2 and Au/TiO_2 hybrid structures. The samples were irradiated under visible light (400-1100 nm): TiO_2 (black curve), Au-on-TiO_2 (blue curve), Au-in-TiO_2-15 (orange curve) and Au-in-TiO_2-270 (red curve). Off corresponds to the dark current. b) Photocurrent-potential curves in 0.05 M Na_2SO_4 solution for TiO_2 (black curve)* and *Au-in-TiO_2 (red curve) obtained under dark and UV+Vis light (353-1100 nm).*

At this point we can discuss the different mechanisms that contribute to the HER under UV+Vis light. Two main mechanisms of surface plasmon resonance can participate when only visible light irradiates on a hybrid metal/semiconductor system:

(i) since under Vis light a readily photocurrent is measured, it can be inferred that, electrons are excited into the TiO_2 to populate the defect states into the gap, at the level of the transferred energy.

(ii) a localized intense oscillating electric field at the Au NPs/semiconductor interface generates hot electrons that are injected into the TiO_2.

In both mechanisms, electrons are thermalized and fast recombination processes take place preventing the electrons migration to the TiO_2 surface to catalyze the photo-reduction of water. This is in accordance with the results showing negligible H_2 production under visible light only.

Under UV + Vis excitation, the energy transfer to the excited electrons in TiO_2 due to SPR is the main proposed mechanism that could explain the observe synergy causing an enhancement of H_2 production. Upon UV irradiation, thermalized and hot photo-excited electrons are being generated, but these are rapidly recombined before reach the surface to catalyze the chemical reaction, this explains the low level of hydrogen produced only under UV. But, when applying visible light, additionally to the injection of hot electrons from Au to the TiO_2 conduction band, the contribution of the intense oscillating electric field at the Au NPs/semiconductor interface, as reported in [45], transfers energy in the range of 2.0 – 2.5 eV, to the existing UV excited electrons in the semiconductor located in the conduction band. These energetic electrons can migrate effectively to the TiO_2 surface and catalyze the chemical reaction. It is important to note that this synergy driven by the plasmonic near field (which increases significantly the number of hot electrons) and the Schottky barrier at the Au/TiO_2 interface (extending the lifespan of the electron), is in accordance with the negative flat band potential observed in the Au-in-TiO_2 nanostructures.

To sum up, the following main steps driving the water splitting process under UV+Vis light is proposed: 1) photo excited electron-hole carriers are generated in TiO_2 (UV light contribution). The Schottky barrier allows charge separation, as photo-excited holes are being attracted by metal NPs where they can be annihilated through recombination. This process is enhanced by the semiconductor crystallinity extending the depletion layer from the metal/semiconductor Schottky contact; 2) surface plasmon resonance create an intense near field in gold nanoparticles (visible light contribution) that transfer energy to existing (UV originated) thermalized electrons in TiO_2, 3) electrons migrate to the semiconductor surface to perform the water splitting reaction.

4. CONCLUSIONS

This study analyses the mechanisms of plasmon-enhanced photocatalytic water splitting and the effect of a metal/semiconductor interface, by characterizing different Au/TiO_2 structures under visible, UV and UV+Vis light. Both experimental data and numerical simulations coherently demonstrate that an important enhancement in the hydrogen production rate is achieved when Au NPs are inside of a TiO_2 film and when visible light is coupled with UV. Moreover, the depth of the Au NPs does not influence significantly the photocatalytic process and hydrogen production rate efficiency if the crystallinity of the semiconductor is high. Results indicate that the essential synergetic role of UV and visible light consists in increasing the carriers lifetimes and on the enhancement of the hot carrier generation in TiO_2, resulting from the energy transfer from the plasmonic field to the photo-excited carriers in TiO_2. Note that, as Au NPs are embedded, the plasmonic near field is more intense and spread over a larger area compared with Au positioned on the top surface. The results also reveal that the water-splitting reaction that leads to H_2 production does not occur on Au NPs, but on the semiconductor surface. Therefore, the TiO_2 crystallinity and

its surface stoichiometry are highlighted as they directly impact the carriers lifetimes and liquid-solid chemical reactions.

ASSOCIATED CONTENT

Supporting Information. The following files are available free of charge: more details in the synthesis and characterization of materials, additional microscopic and XPS characterization, additional photocatalytic experiments, electric field simulations and characterization of the annealed a-Au-in-TiO_2-15 structure.

AUTHOR INFORMATION

Corresponding Author

*(A.E.) E-mail aesteve@laas.fr.

Author Contributions

M.-I. M.-D. and J. C. performed the samples preparation, characterization, H_2 production and electrochemistry measurements. M.-I. M.-D., S.G.P. and D. P. performed the characterization and the photocatalytic tests under filtered light. K. T. performed the XPS characterization. Q.-L. provided support for XPS characterization. T.H. performed the microscopy imaging. C. R. provided support for the manuscript preparation and supervised the research. A. E. realized the simulations, provided support for the manuscript preparation and supervised the research with C. R.

Notes

The authors declare no competing financial interest.

ACKNOWLEDGMENTS

The authors acknowledge the Occitanie Region / European Union for their FEDER support (THERMIE grant) and project support Occitanie Region (MHytyque project). The authors also thank Claudie Josse from the Centre de Microcaractérisation Raimond Castaing for performing the TEM observations and for the preparation of lamellas for SEM observations, respectively. The authors also thank David Gauchard and Ghada Merhaben for providing support to the DDSCAT simulations. The authors also thank Fabien Mesnilgrente, Andréa Nicollet, Séverine Vivies and Ludovic Salvagnac for their assistance in the sputter-deposition development. We finally thank Kevin Cocq for fruitful discussions, notably concerning grafting of nanoparticle issues.

C. Rossi received funding from the European Research Council (ERC) under the European Union's Horizon 2020 research and innovation programme (grant agreement No 832889 - PyroSafe).

REFERENCES

1. Dutta, S., A review on production, storage of hydrogen and its utilization as an energy resource. *J. Ind. Eng. Chem.* **2014,** *20* (4), 1148-1156.
2. Pinaud, B. A.; Benck, J. D.; Seitz, L. C.; Forman, A. J.; Chen, Z.; Deutsch, T. G.; James, B. D.; Baum, K. N.; Baum, G. N.; Ardo, S.; Wang, H.; Miller, E.; Jaramillo, T. F., Technical and economic feasibility of centralized facilities for solar hydrogen production via photocatalysis and photoelectrochemistry. *Energy Environ. Sci.* **2013,** *6* (7), 1983-2002.
3. Prevot, M. S.; Guijarro, N.; Sivula, K., Enhancing the Performance of a Robust Sol-Gel-Processed p-Type Delafossite CuFeO2 Photocathode for Solar Water Reduction. *ChemSusChem* **2015,** *8* (8), 1359-1367.
4. Hisatomi, T.; Kubota, J.; Domen, K., Recent advances in semiconductors for photocatalytic and photoelectrochemical water splitting. *Chem. Soc. Rev.* **2014,** *43* (17), 7520-7535.
5. Wang, Z.; Li, C.; Domen, K., Recent developments in heterogeneous photocatalysts for solar-driven overall water-splitting. *Chem. Soc. Rev.* **2018,** *48* (7), 2109-2125.
6. Maeda, K.; Teramura, K.; Lu, D.; Takata, T.; Saito, N.; Inoue, Y.; Domen, K., Photocatalyst releasing hydrogen from water. *Nature* **2006,** *440* (7082), 295.
7. Wang, X.; Jin, S.; An, H.; Wang, X.; Feng, Z.; Li, C., Relation between the photocatalytic and photoelectrocatalytic performance for the particulate semiconductor-based photoconversion systems with surface phase junction structure. *J. Phys. Chem. C* **2015,** *119* (39), 22460-22464.

8. Goto, Y.; Hisatomi, T.; Wang, Q.; Higashi, T.; Ishikiriyama, K.; Maeda, T.; Sakata, Y.; Okunaka, S.; Tokudome, H.; Katayama, M.; Akiyama, S.; Nishiyama, H.; Inoue, Y.; Takewaki, T.; Setoyama, T.; Minegishi, T.; Takata, T.; Yamada, T.; Domen, K., A Particulate Photocatalyst Water-Splitting panel for Large-Scale Solar Hydrogen Generation. *Joule* **2018,** *2* (3), 509-520.
9. Takata, T.; Domen, K., Particulate Photocatalysts for Water Splitting: Recent Advances and Future Prospects. *ACS Energ. Lett.* **2019,** *4* (2), 542-549.
10. Abdi, F. F.; Han, L.; Smets, A. H. M.; zeman, M.; Dam, B.; Van De Krol, R., Efficient solar water splitting by enhanced charge separation in a bismuth vanadate-silicon tandem photoelectrode. *Nat. Commun.* **2013,** *4*, 2195.
11. Luo, J.; Vermaas, D. A.; Bi, D.; Hagfeldt, A.; Smith, W. A.; Grätzel, M., Bipolar membrane-assisted solar water splitting in optimal pH. *Adv. Energy Mater.* **2016,** *6* (13), 1600100.
12. Ager, J. W.; Shaner, M.; Walczak, K.; Sharp, I. D.; Ardo, S., Experimental demonstrations of spontaneous, solar-driven photoelectrochemical water splitting. *Energy Environ. Sci.* **2015,** *8* (10), 2811-2824.
13. Fujishima, A.; Honda, K., Electrochemical Photolysis of Water at a Semiconductor Electrode. *Nature* **1972,** *238* (5358), 37-8.
14. Kumaravel, V.; Mathew, S.; Bartlett, J.; Pillai, S. C., Photocatalytic hydrogen production using metal doped TiO2: a review of recent advances. *Appl. Catal. B* **2019,** *244*, 1021-1064.
15. Rojas, H. C.; Bellani, S.; Sarduy, E. A.; Fumagalli, F.; Mayer, M. T.; Schreier, M.; Grätzel, M.; Di Fonzo, F.; Antognazza, M. R., All Solution-Processed, Hybrid Organic-Inorganic Photocathode for Hydrogen Evolution. *ACS Omega* **2017,** *2* (7), 3424-3431.
16. Reisner, E.; Powell, D. J.; Cavazza, C.; Fontecilla-Camps, J. C.; Armstrong, F. A., Visible Light-Driven H2 Production by Hydrogenases Atteched to Dye-Sensitized TiO2 Nanoparticles. *J. Am. Chem. Soc.* **2009,** *131* (51), 18457-18466.
17. Watanabe, M.; Sun, S.; Ishihara, T.; Kamimura, T.; Nishimura, M.; Tani, F., Visible Light-Driven Dye-Sensitized Photocatalytic Hydrogen Production by Porphyrin and its Cyclic Dimer and Trimer: Effect of Multi-Pyridyl-Anchoring groups on Photocatalytic Activity and Stability. *ACS Appl. Energy Mater.* **2018**, Ahead of print.
18. Huang, Q.; Tian, S.; Zeng, D.; wang, X.; Song, W.; Li, Y.; Xiao, W.; Xie, C., Enhanced Photocatalytic Activity of Chemically Bonded TiO2/Graphene Composites Based on the Effective Interfacial Charge Transfer through the C-Ti Bond. *ACS Catal.* **2013,** *3* (7), 1477-1485.
19. Coy, E.; Siuzdak, K.; Pavlenko, M.; Zaleski, K.; Graniel, O.; Ziolek, M.; Balme, S.; Miele, P.; Weber, M.; Bechelany, M.; Iatsunskyi, I., Enhancing photocatalytic performance and solar absorption by schottky nanodiodes heterojunctions in mechanically resilient palladium coated TiO2/Si nanopillars by atomic layer deposition. *Chem Eng J* **2020,** *392*.
20. Kawrani, S.; Nada, A. A.; Bekheet, M. F.; Boulos, M.; Viter, R.; Roualdes, S.; Miele, P.; Cornu, D.; Bechelany, M., Enhancement of calcium copper titanium oxide photoelectrochemical performance using boron nitride nanosheets. *Chem Eng J* **2020,** *389*.
21. Livraghi, S.; Paganini, M. C.; Giamello, E.; Selloni, A.; Di Valentin, C.; Pacchioni, G., Origin of Photoactivity of Nitrogen-Doped Titanium Dioxide under Visible Light. *J. Am. Chem. Soc.* **2006,** *128* (49), 15666-15671.
22. Ma, T.; Akiyama, M.; Abe, E.; Imai, I., High-Efficiency Dye-Sensitized Solar Cell Based on a Nitrogen-Doped Nanostructured Titania Electrode. *Nano Lett.* **2005,** *5* (12), 2543-2547.
23. Veziroglu, S.; Ullrich, M.; Hussain, M.; Drewes, J.; Shondo, J.; Strunskus, T.; Adam, J.; Faupel, F.; Aktas, O. C., Plasmonic and non-plasmonic contributions on photocatalytic activity of Au-TiO2 thin film under mixed UV-Visible light. *Surf. Coat. Technol.* **2020**, in press.

24. A., I. A.; Detlef, W. B., One-step synthesis of mesoporous platinium/titania nanocomposites as photocatalyst with enhanced photocatalytic activity for methanol oxidation. *Green Chem.* **2011,** *13*, 428-435.
25. Carneiro, J. T.; Yang, C.-C.; Moma, J. A.; Moulijn, J. A.; Mul, G., How Gold Deposition Affects Anatase Performance in the Photocatalytic Oxidation of Cyclohexane. *Catal. Lett.* **2009,** *129* (1-2), 12-19.
26. Yan, J.; Wu, G.; Guan, N.; Li, L., Synergetic promotion of the photocatalytic activity of TiO2 by gold deposition under UV-visible light irradiation. *Chem. Commun.* **2013,** *49* (100), 11767-11769.
27. Ratchford, D. C.; Dunkelberger, A. D.; Vurgaftman, I.; Owrutsky, J. C.; Pehrsson, P. E., Quantification of Efficient Plasmonic Hot-Electron Injection in Gold Nanoparticle TiO2 Films. *Nano Lett* **2017,** *17* (10), 6047-6055.
28. Seh, Z. W., Liu, S.; Low, M.; Zhang, S.-Y.; Liu, Z.; Mlayah, A.; Han, M.-Y., Janus Au-TiO2 Photocatalysts with Strong Localization of Plasmonic Near-Fields for Efficient Visible-Light Hydrogen Generation. *Adv. Mater.* **2012,** *24* (17), 2310-2314.
29. Silva, C. G.; Juarez, R.; Marino, T.; Molinari, R.; Garcia, H., Influence of Excitation Wavelength (UV or Visible Light) on the Photocatalytic Activity of Titania Containing Gold Nanoparticles for the Generation of Hydrogen or Oxygen from Water. *J. Am. Chem. Soc.* **2011,** *133*, 595-602.
30. Lin, Z.; Wang, X.; Liu, J.; Tian, Z.; Dai, L.; He, B.; Han, C.; Wu, Y.; Zeng, Z.; Hu, Z., On the role of localized surface plasmon resonance in UV-Vis light irradiated Au/TiO2 photocatalysis systems: pros and cons. *Nanoscale* **2015,** *7*, 4114-4123.
31. Okuno, T.; Kawamura, G.; Muto, H.; Matsuda, A., Photocatalytic Properties of Au-Deposited Mesoporous SiO2-TiO2 Photocatalyst under Simultaneous Irradiation of UV and Visible Light. *J. Solid State Chem.* **2016,** *235*, 132-138.
32. Wang, S.; Gao, Y.; Miao, S.; Liu, T.; Mu, L.; Li, R.; Fan, F.; Li, C., Positioning the Water Oxidation Reaction Sites in Plasmonic Photocatalysts. *J. Am. Chem. Soc.* **2017,** *139* (34), 11771-11778.
33. Huang, J. N., W.; Li, C.; Tan, C.; Yin, P.; Cheng, H.; Hu, Z.; Yang, N.; He, Q.; Nam, G.-H.; Zhang, H., In-Situ Probing of Crystal-Phase-Dependent Photocatalytic Activities of Au Nanostructures by Surface-Enhanced Raman Spectroscopy. *ACS Materials Lett.* **2020,** *2* (4), 409-414.
34. Cure, J.; Assi, H.; Cocq, K.; Marin, L.; Fajerwerg, K.; Fau, P.; Beche, E.; Chabal, Y. J.; Esteve, A.; Rossi, C., Controlled Growth and Grafting of High-Density Au Nanoparticles on Zinc Oxide Thin Films by Photo-Deposition. *Langmuir* **2018,** *34* (5), 1932-1940.
35. Cure, J.; Cocq, K.; Mlayah, A.; Hungria, T.; Alphonse, P.; Chabal, Y. J.; Maraval, V.; Chauvin, R.; Esteve, A.; Rossi, C., A triptych photocatalyst based on the co-integration of Ag nanoparticles and carbo-benzene dye into a TiO2 thin film. *Int. J. Hydrogen Energ.* **2019,** *44* (48), 26347-26360.
36. Cure, J.; Cocq, K.; Nicollet, A.; Tan, K.; Hungria, T.; Assie-Souleille, S.; Vivies, S.; Salvagnac, L.; Quevedo-Lopez, M.; Maraval, V.; Chauvin, R.; Esteve, A.; Rossi, C., A Beehive Inspired Hydrogen Photocatalytic Device Integrating a Carbo-Benzene Triptych Material for Efficient Solar Photo-Reduction of Seawater. *Adv Sustain Syst* **2020**.
37. Miquelot, A.; Debieu, O.; Rouessac, V.; Villeneuve, C.; Prud'homme, N.; Cure, J.; Constantoudis, V.; Papavieros, G.; Roualdes, S.; Vahlas, C., TiO2 nanotree films for the production of green H2 by solar water splitting: From microstructural and optical characteristics to the photocatalytic properties. *Appl. Surf. Sci.* **2019,** *494*, 1127-1137.
38. Kruse, N.; Chenakin, S., XPS characterization of Au/TiO2 catalysts: Binding energy assesment and irradiation effects. *Appl. Catal. A* **2011,** *391* (1-2), 367-376.
39. Wang, T. M.; Zheng, S. K.; Hao, W. C.; Wang, C., Studies on photocatalytic activity and transmittance spectra of TiO2 thin films prepared by r.f. magnetron sputtering method. *Surf. Coat. Tech.* **2002,** *155*, 141-145.

40. Schlather, A. E.; Manjavacas, A.; Lauchner, A.; Marangoni, V. S.; De Santis, C. J.; Nordlander, P., Halas, N. J., Hot Hole Photoelectrochemistry on Au@SiO2@Au Nanoparticles. *J. Phys. Chem. C* **2017,** *8* (9), 2060-2067.
41. Zhou, L.; Swearer, D. F.; Zhang, C.; Robatjazi, H.; Zhao, H.; Henderson, L.; Dong, L.; Christopher, P.; Carter, E. A.; Nordlander, P.; Halas, N. J., Quantifying hot carrier and thermal contributions in plasmonic photocatalysis. *Science* **2018,** *362* (6410), 69-72.
42. Lin, L.; Ma, Y.; Wu, J.; Pang, F.; Ge, J.; Sui, S.; Yao, Y.; Qi, R.; Cheng, Y.; Duan, C.-G.; Chu, J.; Huang, R., Origin of Photocatalytic Activity in Ti4+/Ti3+ Core-Shell Titanium Oxide Nanocrystals. *J. Phys. Chem. C* **2019,** *123*, 20949-20959.
43. Dwivedi, N.; Yeo, R. J.; Tan, H. R.; Stangl, R.; Aberle, A. G.; Bhatia, C. S.; Danner, A.; Liao, B., Evidence for Chemicals Intermingling at Silicon/Titanium Oxide (TiOx) Interface and Existence of Multiple Bonding States in Monolithic TiOx. *Adv. Funct. Mater.* **2018,** *28*, 1707018.
44. Lei, J. F.; Li, X. P.; Li, W. S.; Sun, F. Q.; Lu, D. S.; Yi, J., Arrayed porous iron-doped TiO2 as photoelectrocatalyst with controllable pore size. *Int J Hydrogen Energ* **2011,** *36* (14), 8167-8172.
45. Khan, M. R.; Chuan, T. W.; Yousuf, A.; Chowdhury, M. N. K.; Cheng, C. K., Schottky barrier and surface plasmonic resonance phenomena towards the photocatalytic reaction: study of their mechanisms to enhance photocatalytic activity. *Catal Sci Technol* **2015,** *5* (5), 2522-2531.

TOC Graphic

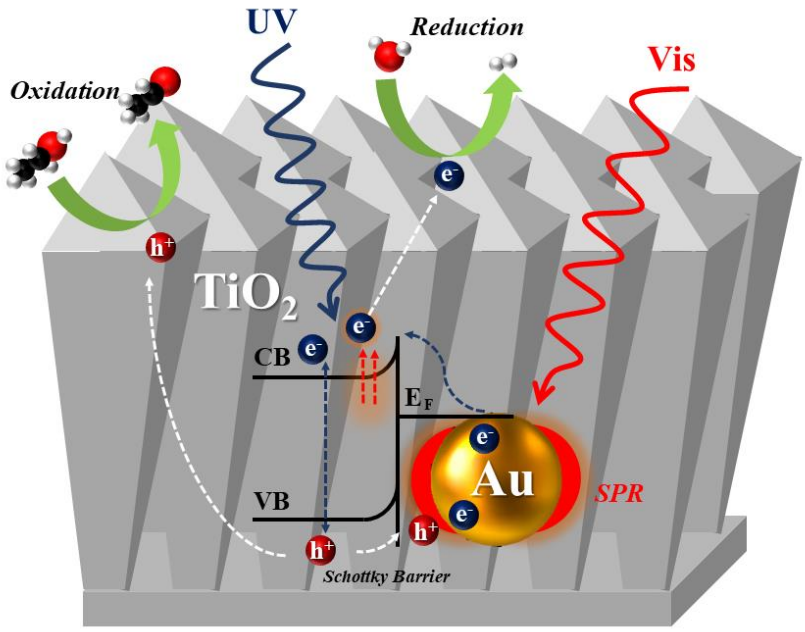
UV
Reduction
Vis
Oxidation
TiO2
CB
VB
EF
Au
SPR
Schottky Barrier